Electronic Supplementary Information

Order-Disorder Transition in the *S* = ½ Kagome Antiferromagnets Claringbullite and Barlowite

Alyssa Henderson, Lianyang Dong, Sananda Biswas, Hannah I. Revell, Yan Xin, John A. Schlueter, Roser Valenti, and Theo Siegrist**

Table of Contents

Experimental Procedures

Synthesis

Hydrothermal reactions were performed by combining CuO (6 mmol, 477 mg), CuF_2 (1 mmol, 102 mg), and $CuCl_2{\cdot}2H_2O$ (1 mmol, 170 mg or 0.5 mmol 86 mg) or $CuBr_2$ (1 mmol, 220 mg or 0.5 mmol, 110 mg) in 23 mL Parr General Purpose Acid Digestion Vessels, for claringbullite and barlowite respectively. It was found that less $CuCl_2{\cdot}2H_2O$ would often yield larger single crystals. The contents of the autoclave were heated for 100 hours at 150 °C, cooled to room temperature over 24 hours. The result in both cases was an aqua blue mixture at the bottom of the vessel, which was poured onto filter paper, dried, and collected. Both barlowite and claringbullite powder and single crystals were synthesized within each respective reaction.

Larger single crystals of claringbullite were prepared through use of seed crystals, as described earlier.[1] In a typical reaction, a mixture of $CuO:CuF_2:CuCl_2$ in a 6:1:1 molar ratio was placed in a 23 ml Parr vessel with 15 mL of water. Seed crystals were added to the vessel, which was then heated at 170 °C for 72 hours. Repeating this process over seven cycles resulted in the growth of crystals larger than 0.5 mm.

In order to prepare polycrystalline powders of claringbullite, a solution method was developed. In a Teflon cup, NH_4F (8 mmol, 133.8 mg) and NaOH (6 mmol, 108.4 mg) were dissolved in 20 mL water. In a second cup, $CuCl_2{\cdot}2H_2O$ (4 mmol, 308 mg) was dissolved in 10 mL water. Upon combination, 163.7 mg (29.6% yield) of claringbullite polycrystalline powder formed. The claringbullite powder was subsequently separated from the water via filtration, and dried in an oven at 30 °C.

Table 1. Details of starting stoichiometry of single crystals studied using the APS ChemMatCARS beamline.

Sample	CuO	CuF_2	$CuCl_2{\square}2H_2O$	Temp, time	mL
C_01	6mmol, 473 mg	1mmol, 101 mg	½ mmol, 85 mg	150C, 100h	20
C_02	6mmol, 477 mg	1mmol, 100 mg	1mmol, 170 mg	150C, 100h	19
C_28	6mmol, 476 mg	1mmol, 101 mg	½ mmol, 86 mg	150C, 100h	20
B_05	6mmol, 480 mg	1mmol, 101 mg	CuBr: ½ mmol, 114mg	150C, 100h	20

[1] C. M. Pasco, B. A. Trump, T. T. Tran, Z. A. Kelly, C. Hoffmann, I. Heinmaa, R. Stern, T. M. McQueen, *Physical Review Materials* **2018**, *2*, 044406.

Structural Characterization

Powder X-ray diffraction. Structural studies were carried out on polycrystalline materials through use of a Scintag PAD-V powder diffractometer with diffracted beam monochromator, Further room temperature structural studies used the mail-in program at the Advanced Photon Source (APS) beam line 11-BM for powder diffraction.

Single-crystal x-ray diffraction. The structure of single crystals were analyzed using an Oxford Diffraction Xcalibur-2 CCD diffractometer with graphite monochromated MoKα radiation and a Croyjet temperature control system operating in the range of 110 to 300 K to collect integrated intensities for structural refinements., A custom 4-circle Huber diffractometer in triple axis mode using graphite monochromators was used to follow specific reflection profiles and intensities in the temperature range of 200 to 300 K.

Structural characterization of microcrystals of barlowite and claringbullite were performed at both 10 K and 100 K at the ChemMatCARS sector 15 beamline of the Advanced Photon Source (APS) using a wavelength of 0.41328 Å, through use of a Bruker D8 diffractometer equipped with a PILATUS3 X CdTe 1M detector. Details of starting stoichiometry of single crystals studied are shown in Table S1. The structure of claringbullite sample C_01 was solved at 100 K and refinement details are shown in Tables S2-S4. Additional twinning was present in the same sample at a temperature of 10 K.

Other space groups were considered based on subgroups of P63/mmc and *Cmcm*. Unbiased structure solution in P1 resulted in atom positions consistent with *Pnma*.

Electron microscopy studies. The claringbullite structure was analyzed through use of atomic resolution high angle annular dark field scanning transmission electron microscopy (HAADF-STEM) with a probe-aberration-corrected cold field-emission JEOL JEM-ARM200cF microscope operating at 200 kV at room temperature, with a current of 21 pA. The STEM resolution of the microscope is 0.78 Å. The images were taken with a probe size of 0.078 nm, a condense lens aperture aperture of 30 μm, scan speed of 32 μs/pixel, and camera length 8 cm, which corresponds to a probe convergence angle of 21 mrad and collection angle of 78.6 mrad. The TEM sample was prepared by grinding and depositing the powder on a carbon coated 200 μm mesh TEM Cu grid.

Table 2: Structural refinement information for x-ray diffraction data collected on claringbullite crystal C_01 at the ChemMatCARS beamline.

Structure	
Formula	$Cu_4(OH)_6FCl$
Symmetry	*Pnma* #62
a	11.5133(2) Å
b	9.1527(2) Å
c	6.6727(2) Å
Z	4
Volume	703.144(2) Å^3
Reflections total	28695
Reflections unique	2016
θ_{min}	2.05°
θ_{max}	22.19°
$\lambda(synchrotron)$	0.41328
R_{all}	0.094
wR_{obs}	0.071

Table 3: Atomic positions and U_{eq} [Å^2]

atom	type	x	y	z	Ueq
Cu1	Cu	0.5000	0.5000	0.0000	0.0050
Cu2	Cu	0.75074(2)	0.51320(3)	0.24494(4)	0.0047
Cu3	Cu	0.31467(4)	0.7500	−0.05897(7)	0.0070
O4	O	0.60259(15)	0.40922(18)	0.1996(3)	0.0042
O5	O	0.40195(15)	0.58806(19)	0.1981(3)	0.0044
O6	O	0.69984(19)	0.59573(19)	0.5021(3)	0.0069
Cl7	Cl	0.67227(9)	0.7500	0.00919(14)	0.0095
F8	F	0.5023(2)	0.7500	−0.4938(4)	0.0082

Table 4: Anisotropic thermal parameters [Å^2]

atom	u11	u22	u33	u23	u13	u12
Cu1	0.00180(17)	0.00594(19)	0.00723(19)	0.00042(13)	0.00015(12)	0.00184(15)
Cu2	0.00184(12)	0.00507(13)	0.00731(14)	−0.00218(10)	−0.00012(9)	−0.00097(10)
Cu3	0.00511(18)	0.00250(17)	0.0133(2)	0.0000	0.00257(16)	0.0000
O4	0.0013(6)	0.0049(7)	0.0064(8)	−0.0002(5)	0.0010(5)	0.0007(5)
O5	0.0017(7)	0.0072(7)	0.0044(7)	−0.0017(5)	0.0004(5)	−0.0003(5)
O6	0.0079(9)	0.0012(7)	0.0116(8)	−0.0004(5)	−0.0007(5)	0.0002(6)
Cl7	0.0107(4)	0.0041(3)	0.0136(4)	0.0000	−0.0001(3)	0.0000
F8	0.0024(9)	0.0074(10)	0.0148(10)	0.0000	0.0011(6)	0.0000

CCDC 1882561 (claringbullite, *Pnma*, temperature 100K, single crystal), 1883264 (claringbullite, *$P6_3/mmc$,* temperature 295K, powder), 1883276 (barlowite, *$P6_3/mmc$,* temperature

295K, powder), and 1019246 (barlowite, temperature 295K, single crystal) contain the supplementary crystallographic data for this paper. These data are provided free of charge by The Cambridge Crystallographic Data Centre.

Ab-initio Calculations

Total-energy calculations are performed using density functional theory (DFT) method as implemented in VASP [1]. The projector-augmented wave method is used with an energy cutoff of 650 eV. The exchange-correlation functional is approximated with the generalized gradient approximation (GGA) and Dudarev's scheme [2] is used to include correlation corrections with an effective correlation strength of *U*eff = 5 eV. K-point meshes of size 8×8×6 and 8×5×6 are used for the room-temperature (P63/*mmc* unit cell) and low-temperature (*Cmcm* unit cell) structures, respectively, both for barlowite and claringbullite. For our calculations with *Pnma* symmetry, we have used the similar k-point mesh as used for *Cmcm*. Figure S11 illustrates the geometry used.

[1] Kresse G. and Hafner J., *Ab initio molecular dynamics for liquid metals* Phys. Rev. B **47**, 558 (1993). doi: https://link.aps.org/doi/10.1103/PhysRevB.47.55

[2] Dudarev S. L., Botton G. A., Savrasov S. Y., Humphreys C. J., and Sutton A. P., *Electron-energy-loss spectra and the structural stability of nickel oxide: An LSDA+U study* Phys. Rev. B **57**, 1505 (1998). doi: https://link.aps.org/doi/10.1103/PhysRevB.57.1505

Supplemental Figures

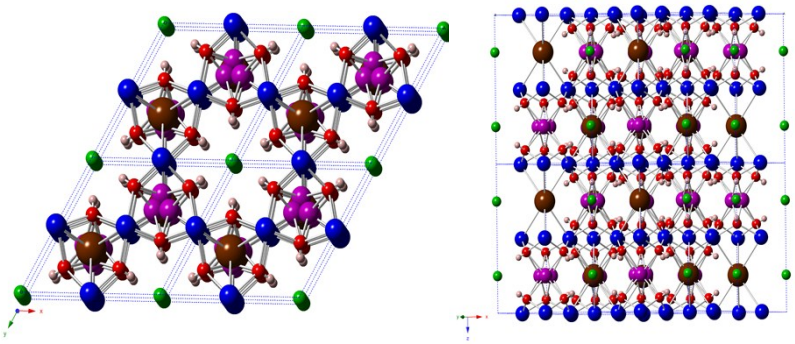

Figure 1. Packing diagram of barlowite, $Cu_4(OH)_6FBr$. Color scheme: Cu (Kagome layer) = blue, Cu (interlayer) = purple, O = red, H = salmon, Br = brown, F = green. (left) Illustration of the layer viewed along the *c*-axis. (right) Illustration of the layer packing. Claringbullite, $Cu_4(OH)_6FCl$, is isostructural, with the bromide ions replaced with chloride.

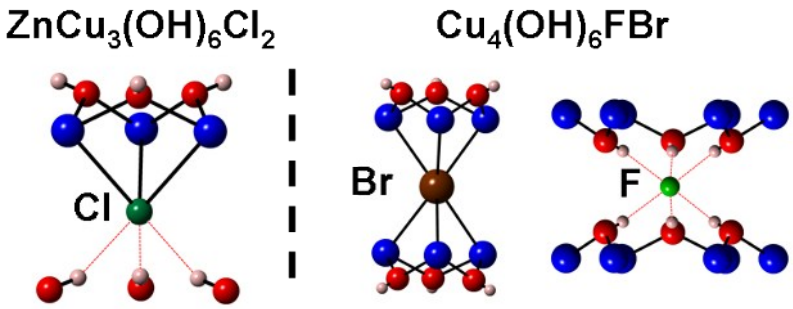

Figure 2. (left) The coordination environment of the interlayer chloride site in herbertsmithite. (right) Two distinct halogen sites in barlowite. Color scheme: Cl = dark green, Cu = blue, O = red, H = salmon, Br = brown, and F = light green.

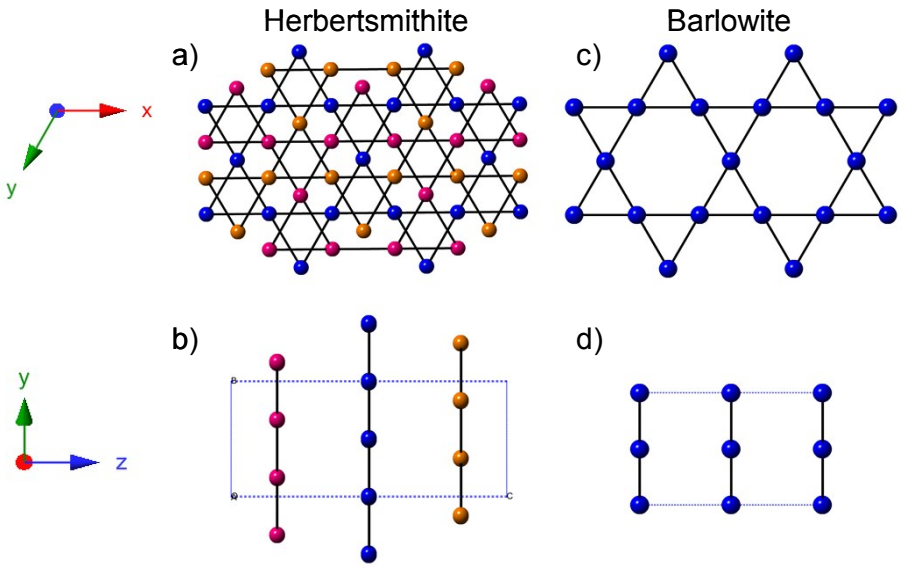

Figure 3. Different stackings of kagome layers. In herbertsmithite (a,b), there are three layers per unit cell along the *c*-axis. For clarity, the copper sites in adjacent layers are illustrated in different colors. In barlowite and claringbullite (c,d), the kagome layers reside directly above each other along the *c*-axis.

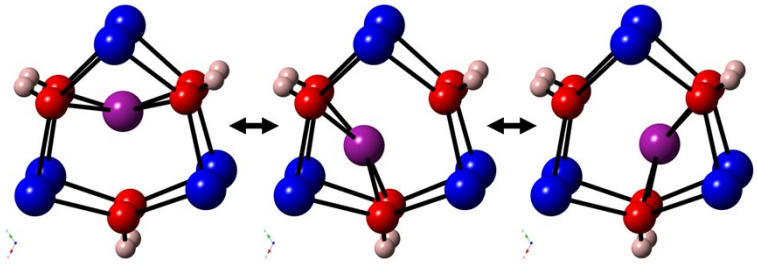

Figure 4. The three possible coordination modes of the interlayer copper site. Above the lock-in temperature, the copper ion fluctuates among these three sites. Purple: copper (interlayer), Blue: copper (kagome), Red: oxygen, Salmon: hydrogen. Above the lock-in temperature, the copper ion fluctuates among these three sites.

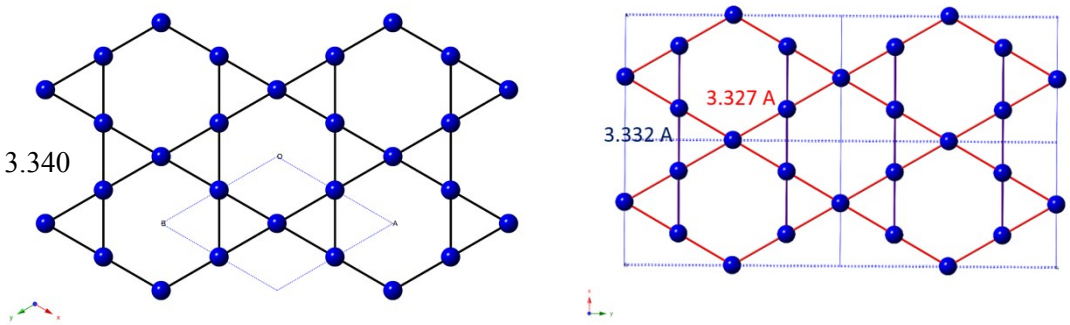

Figure 5. (Left) At room temperature, barlowite crystallizes in the hexagonal *P6$_3$/mmc* space group and has a prefect kagome lattice. (Right) As the temperature is lowered, a distortion to the orthorhombic *Cmcm* space group is observed, with a corresponding distortion in the kagome layer.

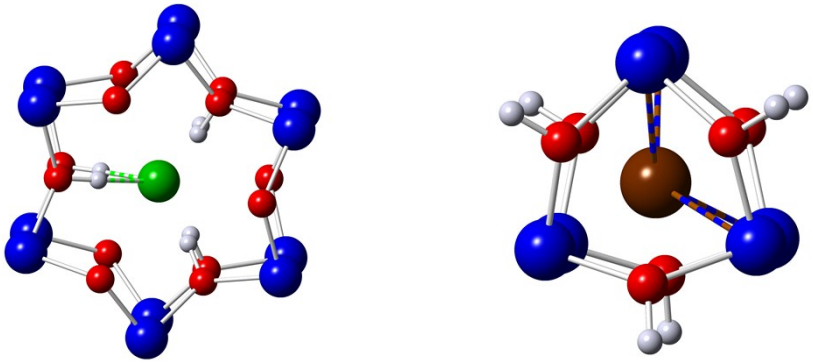

Figure 6. In the low temperature orthorhombic structure, the fluoride ion forms two hydrogen bonds (shown) of 1.737 A. The remaining four H-F interactions expand to 1.829 A. In the orthorhombic structure, the bromide anion also chooses one of three possible coordination environments, with four short (3.007 A) and two long (3.011 A) Cu-Br bonds.

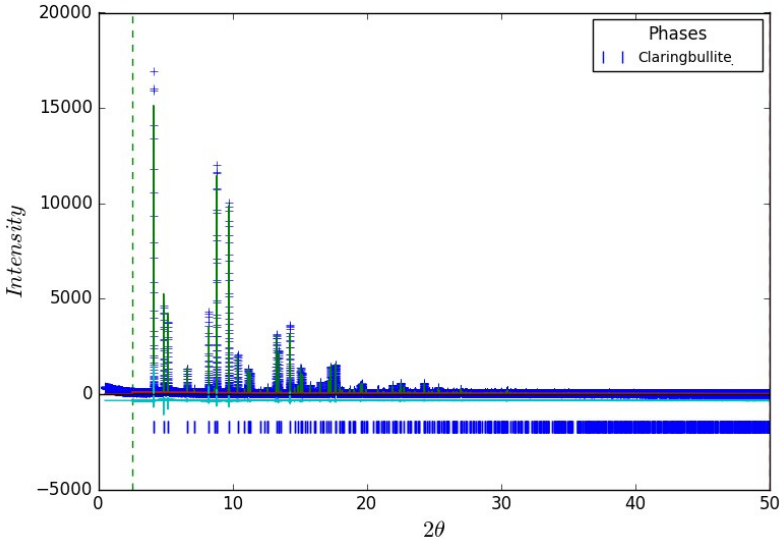

Figure 7. APS X-ray powder diffraction data for claringbullite at ambient temperature with GSAS-II refinement.

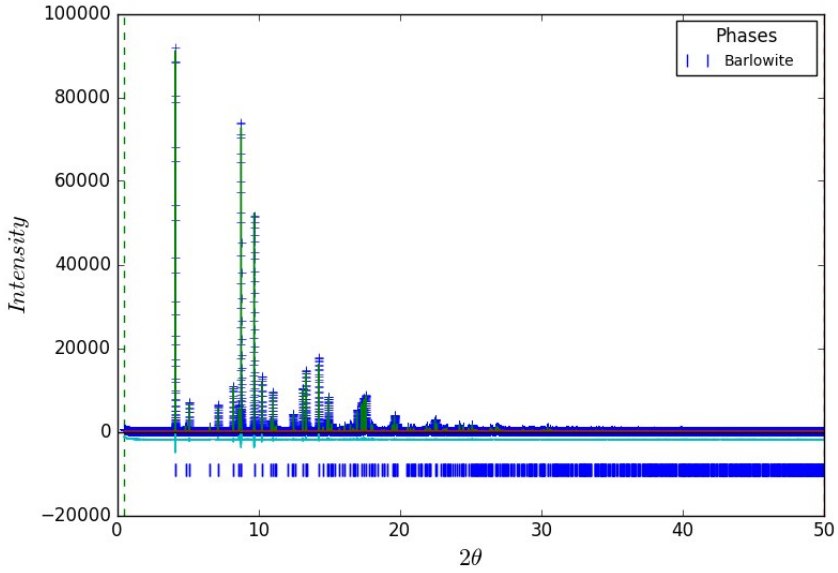

Figure 8. APS X-ray powder diffraction data for barlowite at ambient temperature with GSAS-II refinement.

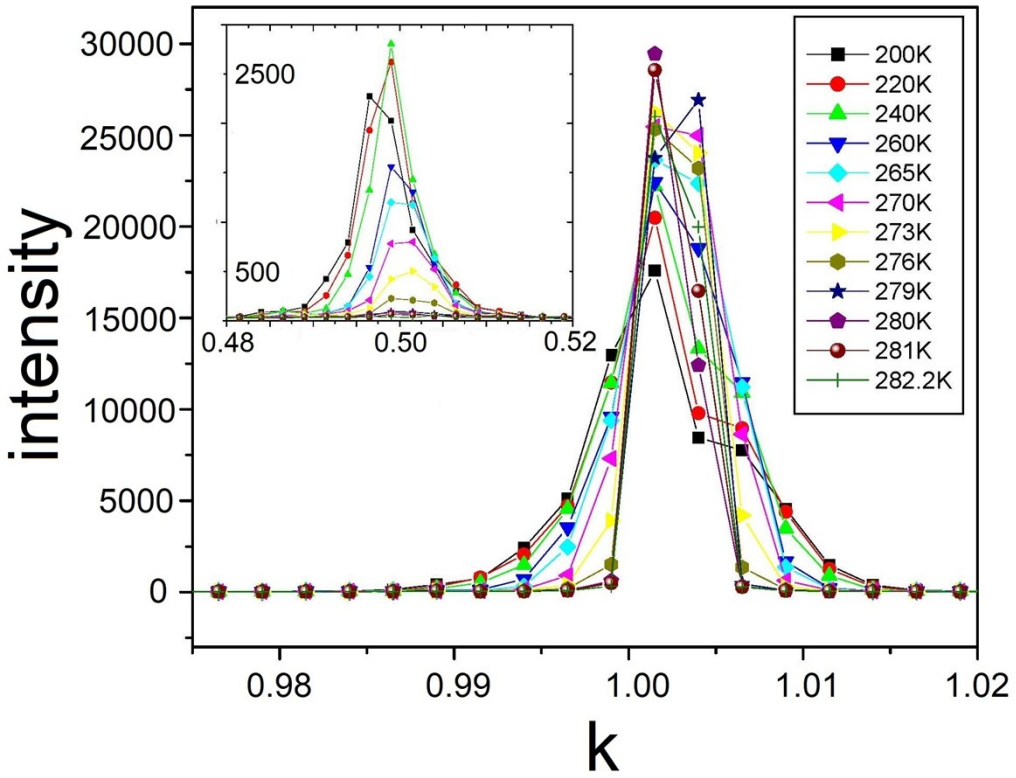

Figure 9. k and T dependence of the intensity of the substructure reflection (-2, 1, 0) and superstructure reflection (-2, 0.5, 0) (inset) for a single crystal of barlowite. The peak broadening of the substructure reflection can be seen.

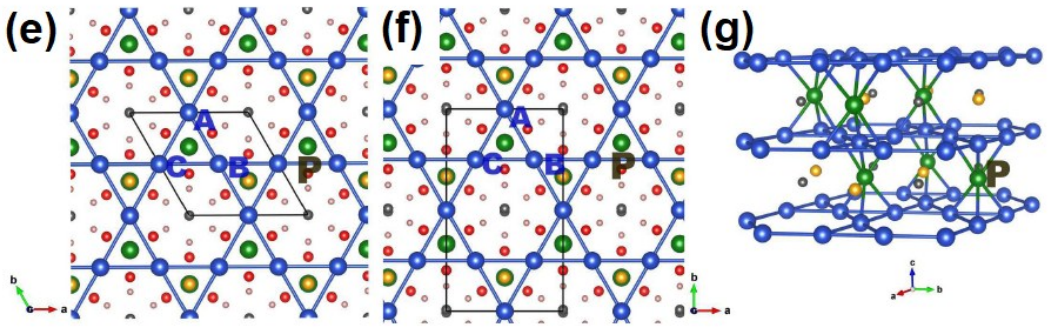

Figure 10. Top views of the Kagome planes in barlowite in *P6₃/mmc* (e) and *Cmcm* (f) geometry. The blue and green atoms are the Cu atoms belonging to the Kagome (blue atoms) and interlayer plane (green atoms), respectively. (g) shows the side view of Cu network. The unit-cell used for calculation is shown by the black lines. Note here that the interlayer Cu atoms were placed at the (hypothetical) highly symmetric position P in order to explain the potential energy surface (PES) later. A, B and C denote the projection of the three nearest Cu ions on the Kagome layer on the plane containing P. Grey, yellow, red and pink spheres indicate F, Cl/Br, O and H atoms.

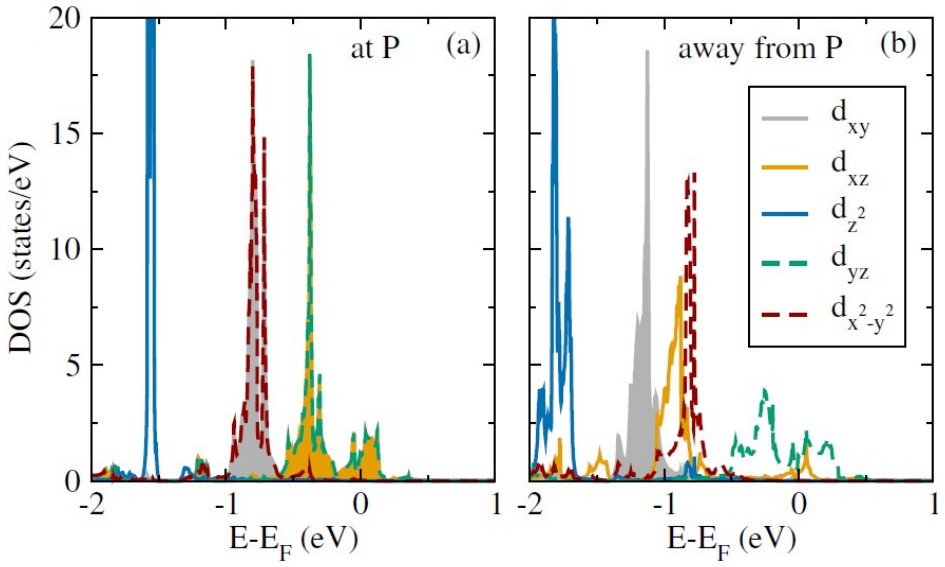

Figure 11. *l*-decomposed partial density of state (DOS) of interlayer Cu^{2+} ion in barlowite (a) at position P and (b) when away from P. The results suggest that these materials undergo a 'Jahn-Teller like distortion' due to the instability caused by the electronic degeneracy between two sets of d-orbitals of the interlayer Cu^{2+} ion at the position P with point group symmetry C_{3v} (Figure S11a). Thus, the system becomes unstable with respect to the nuclear motion away from P in such a way that this degeneracy is lifted; this is evident from Figure S11b.